Supplementary Information

Anisotropic superhydrophobic graphene aerogel with radial superelasticity and axial superstiffness for efficient on-demand oil-water separation

Yu Yang[a,b], Zhiying Ren[a,b,*], Chunhui Zhou[a,b], Youxi Lin[a,b], Linwei Shi[a,b], Linxi Hou[c, d,*]

---

[a]*College of Mechanical Engineering and Automation, Institute of Metal Rubber & Vibration Noise, Fuzhou University, Fuzhou 350116, People's Republic of China.*

[b]*Fuzhou Friction and Lubrication Industry Technology Innovation Center, Fuzhou 350116, People's Republic of China.*

[c]*Department of Materials-Oriented Chemical Engineering, College of Chemical Engineering Fuzhou University, Fuzhou 350116, People's Republic of China.*

[d]*Qingyuan Innovation Laboratory, Quanzhou, 362801, China.*

*E-mail: renzyrose@126.com (Ren); lxhou@fzu.edu.cn (Hou)

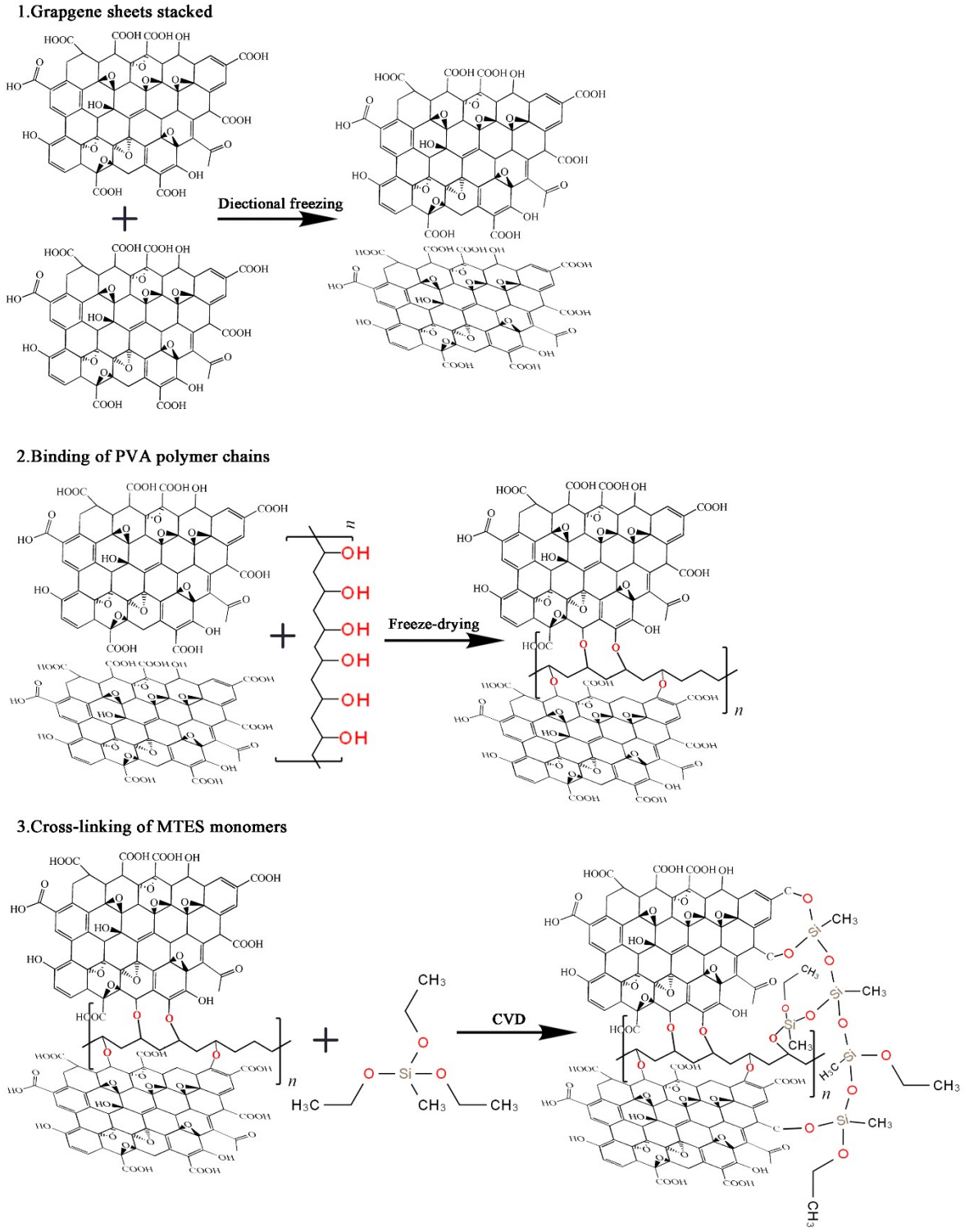

Fig. S1 the reaction schematic of the stacking state of graphene sheets, the combination of PVA polymer chains with graphene sheets, and the cross-linking of MTES monomers.

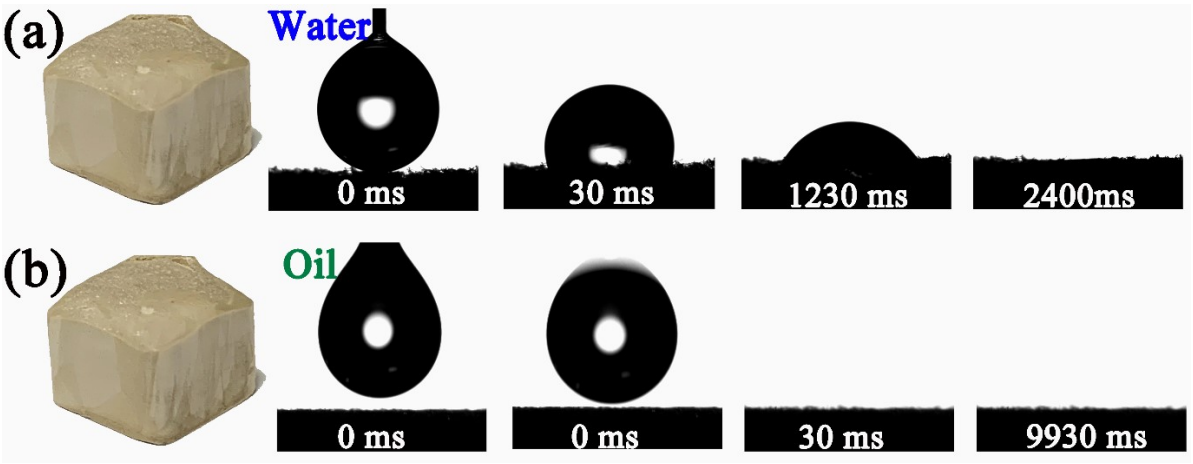

Fig. S2 The wettability of the sample (GPA) without MTES crosslinking. (a) Dynamic wetting behavior of water on GPA. (b) Dynamic wetting behavior of oil on GPA.

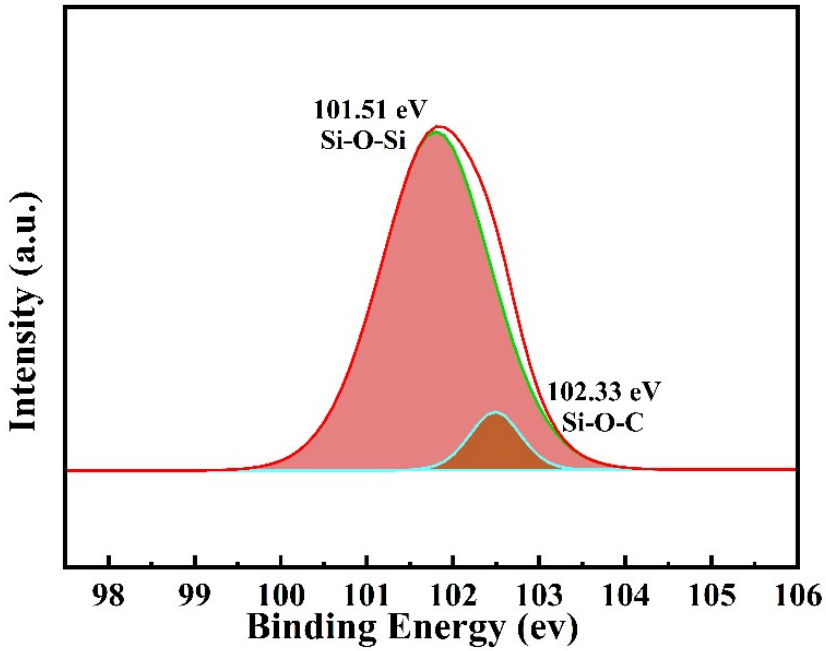

Fig. S3 High-resolution XPS Si 2p spectra of the Si-GPA.

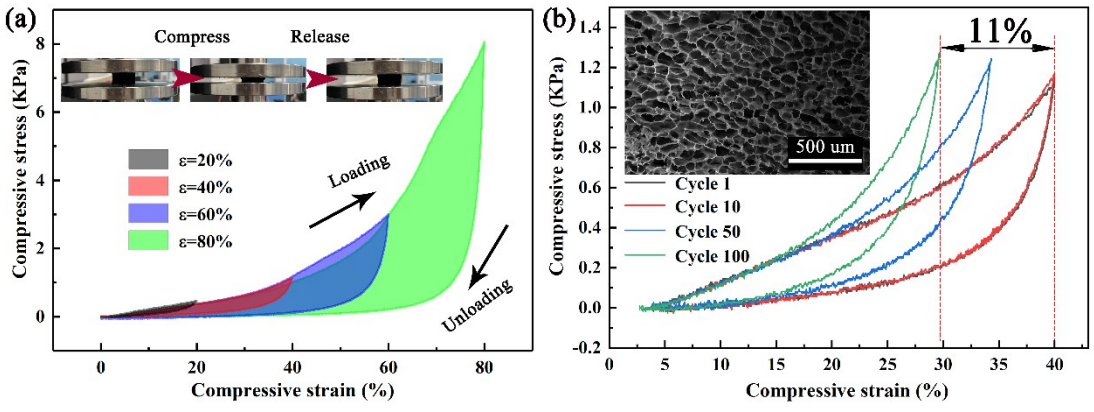

Fig. S4 Hysteresis curves of GPA prepared by non-vertical freeze-drying methods. (a) Compressive stress−strain cycles of GPA with maximum strains of 20, 40, 60, and 80% in succession. Insets: Snapshots of GPA under compression−release cycle (ε = 80%). (b) Cyclic compressive stress−strain curves of GPA at 40% maximum strain for 1, 10, 50, 100 cycles. Insets: internal SEM of GPA after 100 times compression.

The hysteresis curves of aerogels prepared by non-vertical freeze-drying methods, as shown in Fig. S4, do not differ much from those of Si-GPA for 20% to 80% compression. However, the difference in durability is huge, with the deformation of GPA exceeding 10% after 100 cycles, whereas the shape of Si-GPA remains basically unchanged even after 50,000 cycles of compression. It can also be seen from the inset that the aperture of the sample with non-vertical freezing is also without a deterministic shape.

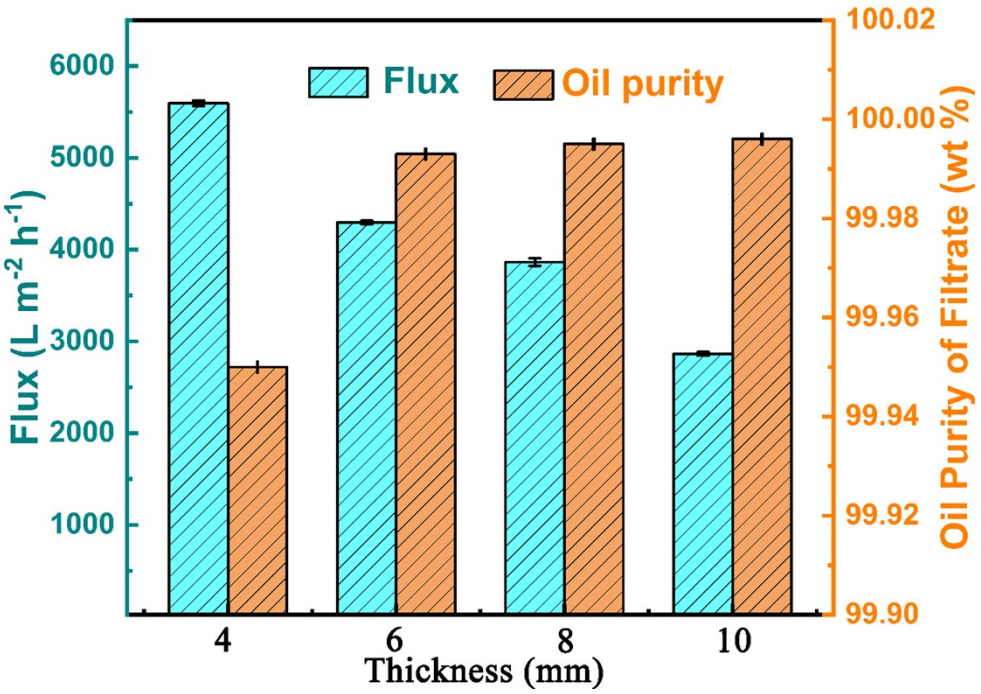

Fig. S5 Thickness of Si-GPA as a function of flux and efficiency

As shown in Figure S5, the filtration flux decreased with the increasing height of the Si-GPA sample, while the oil purity increased initially and then stabilized. At a height of 6 mm, the oil purity reached over 99.99%, but it remained nearly constant above 6 mm. Therefore, we chose a 6 mm-high Si-GPA sample as the oil-water filtration material, retaining both high flux and high precision.

Table S1 Comparison of emulsions separation performance between our work with other representative 2D superwetting oil-water separation materials in 2023.

Material	Fabrication methods	Emulsion types	Flux (L/ m^2 h)	Pressure	Efficiency (%)	Reference /Year
Silane-crosslinked graphene oxide/polyvinyl alcohol aerogel	freeze-drying and chemistry vapor deposition (CVD)	water-in-oil	4350	gravity	99.9%	This work
Stainless steel mesh	growing hierarchical cobalt phosphide arrays	oil-in-water emulsions	2248	0.1bar	99.10%	1
Electro-Fenton assisted superhydrophilic membrane	Partial hydrophilic modification	Oil-in-water emulsion	2258	gravity	99.9%	2
Janus polyacrylonitrile nanofiber membranes	carbon nanotubes (CNTs) doped with PAN	water-in-oil emulsion	2188	gravity	99.8%	3
Superhydrophobic fiberglass (FG) membrane	Dodecyltrimethoxysilane (DTMS)-modified TiO2	water-in-oil emulsion	3130	gravity	99.0%	4
SiO2/PDA@CuC2O4 membrane	bridging polydopamine	Oil-in-water emulsion	2500	gravity	99.7%	5
Ag@sPEN nanofibrous membranes	electrospun	Oil-in-water emulsion	3597	0.09mPA	99.0%	6
Cellulose ester (MCE) membrane	spray	Oil-in-water emulsion	1555	gravity	99%	7
Polytetrafluoroethylene nanofibrous membrane	shear-induced in-situ fibrillation	water-in-oil emulsion	1744	1.5bar	99.9%	8
Polyethylene terephthalate fiber membrane	electrostatic spinning, in-situ deposition and surface modification	water-in-oil emulsion	1100	gravity	99.5	9
PAAm-TA hydrogel coated PVDF membranes	coated	Oil-in-water emulsion	1184	gravity	99.47	10
Palm skin membrane	freezing and salting out strategy	oil-in-water emulsion	1298	gravity	99.9	11
PTFE@ZIF-8 fibrous membrane	electrospun	water-in-oil emulsion	2157	gravity	99.5	12
PVDF membrane	in-situ growth of sliver nanoparticles	Oil-in-water emulsion	2357	gravity	99.4	13
Janus silicon carbide membrane	emerging reactive sintering method	water-in-oil emulsion	1910	gravity	99.3	14
Superhydrophobic/ superoleophilic surface	double depositions of SiO2-TiO2 nanoparticles	oil-in-water emulsion	3000	gravity	99.2	15

CFD Simulation:

Table S2 Physical parameters of fluids.

Fluids	Density (kg/m^3)	Viscosity ($kg/(m\cdot s)$)	Volume ratio	Interfacial tension(N/M)	Contact angle
water	998.2	0.001	1	0.072(air)	152°（under air）
n-hexane	660.0	0.0003	64	0.032(n-hexane)	0°（under air）
air	1.205	1.79×10^{-5}	35	0.02(n-hexane)	0° (under oil)

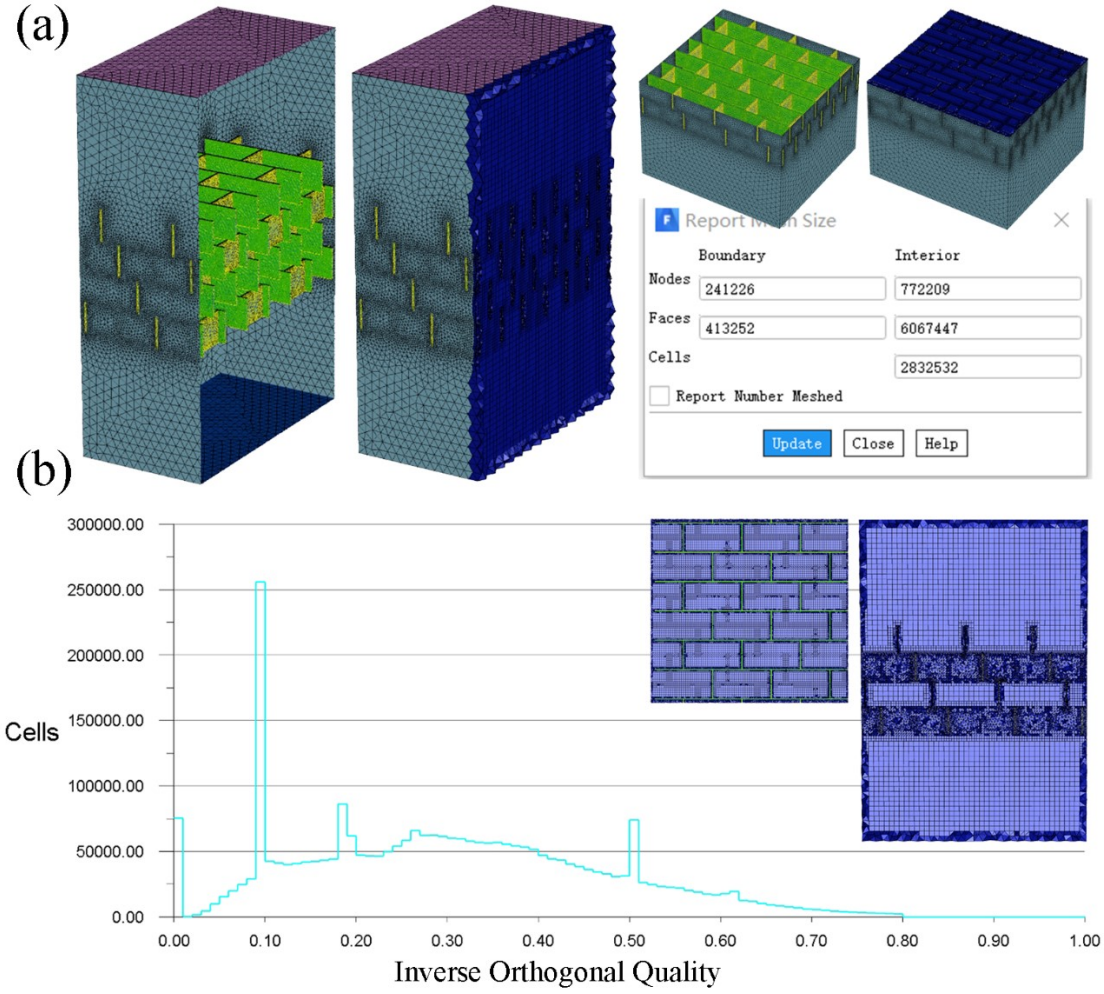

Fig. S6 Mesh model. (a) Face mesh and body mesh sectional views, and mesh count chart, (b) Inverse orthogonal quality chart (The inset is a straight view of the mesh section).

1.Method for interfacial tension force

The continuum surface force (CSF) model was proposed by Brackbill. Interprets surface tension as a continuous, three-dimensional effect across an interface, rather than as a boundary value condition on the interface. Surface tension effects are modeled by the addition of a source term in the momentum equation. To understand the origin of the source term, consider the special case where surface tension is constant along the surface, and where only the forces normal to the interface are considered. The pressure drop across the surface depends upon the surface tension coefficient, σ, and the surface curvature as measured by two radii in the orthogonal directions, R_1 and R_2:

$$p_2 - p_1 = \sigma(\frac{1}{R_1} + \frac{1}{R_2}) \tag{1}$$

where p_1 and p_2 are the pressures in two fluids on either side of the interface.

The surface curvature was computed from the local gradients in the surface normal at the interface. Let n be the surface normal, defined as the gradient of α_q, the volume fraction of the q^{th} phase.

$$n = \nabla \alpha_q \tag{2}$$

The curvature, κ, is defined in terms of the divergence of the unit normal, $\hat{n}$

$$\kappa = \nabla \hat{n} \tag{3}$$

$$\hat{n} = \frac{n}{|n|} \tag{4}$$

Surface tension can be written in terms of pressure jump across the surface. The force at the surface can be expressed as a volume force using the divergence theorem. This volume force is a source term in the momentum equation, and is expressed as:

$$F_{sf} = F_{vol} = \sigma_{ij} \frac{\rho \kappa_i \nabla \alpha_i}{\frac{1}{2}(\rho_i + \rho_j)} \tag{5}$$

where ρ is the volume-averaged density.

2. Method for describing wettability

To describe the wettability on the membrane surface, a method developed by Sussman was employed. The interface represented by VOF function C was extrapolated into the membrane wall ensuring that the specified contact angle was satisfied (Fig. S7):

$$\frac{\partial C}{\partial \tau_2} + u_{extend} \nabla C = 0 \tag{6}$$

Here, τ_2 is the pseudo time and set at $0.5\,\Delta x$, and u_{extend} is the extended velocity.

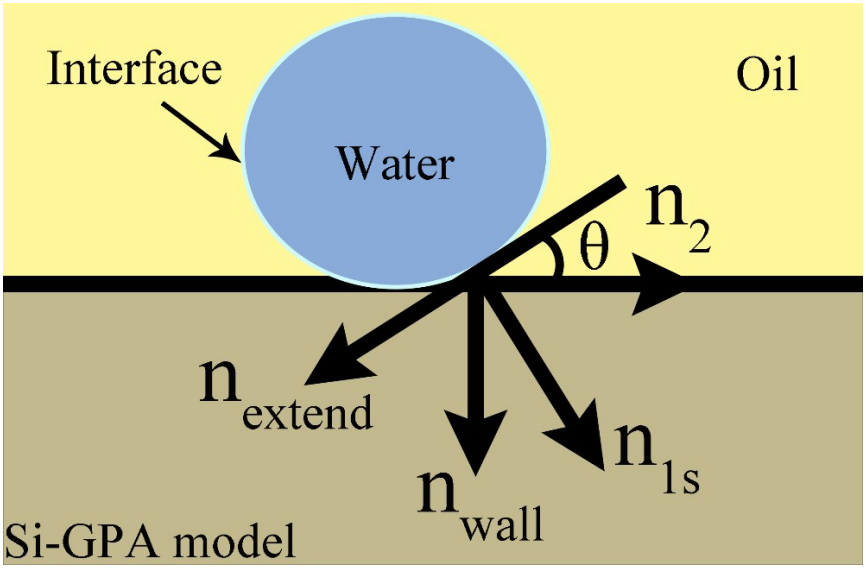

Fig. S7 Schematic diagram of a method for describing wettability.

References

1. H. Li, J. Zhang, S. Gan, X. Liu, L. Zhu, F. Xia, X. Luo and Q. Xue, *Advanced Functional Materials*, 2023, DOI: 10.1002/adfm.202212582.
2. L. Wang, J. Niu, S. Gao, Z. Liu, S. Wu, M. Huang, H. Li, M. Zhu and R. Yuan, *Journal of Membrane Science*, 2023, **670**.
3. X. Yan, Y. Wang, Z. Huang, Z. Gao, X. Mao, M. J. Kipper, L. Huang and J. Tang, *ACS Applied Nano Materials*, 2023, **6**, 4511-4521.
4. J. Li, S. Huang, L. Zhang, H. Zhao, W. Zhao, C. Yuan, X. J. S. Zhang and P. Technology, 2023, **313**, 123480.
5. Y. Liu, H. He, T. J. Zhang, T. C. Zhang, Y. Wang and S. Yuan, *J Hazard Mater*, 2023, **451**, 131142.
6. X. Li, X. He, Y. Ling, Z. Bai, C. Liu, X. Liu and K. Jia, *Journal of Membrane Science*, 2023, **675**.
7. Y.-J. Yeh, J. P. Chu, J.-D. You, T.-H. Chang, J. R. Liou, W.-H. Chiang, P. Yiu, C.-H. Hsueh, Y.-L. Shen and K.-L. Tung, *npj Clean Water*, 2023, **6**.
8. J. Chai, G. Wang, A. Zhang, X. Li, Z. Xu, J. Zhao and G. Zhao, *Chemical Engineering Journal*, 2023, **461**.
9. H. Chen, Z. Zuo, Q. Tian, S. Xue, F. Qiu, X. Peng and T. Zhang, *Journal of Cleaner Production*, 2023, **396**.
10. Y. Jiang, C. Xian, X. Xu, W. Zheng, T. Zhu, W. Cai, J. Huang and Y. J. J. o. M. S. Lai, 2023, **667**, 121166.
11. M. Xia, J. Gao, M. Cai, J. Li, X. Cao, H. Liu, Y. J. S. Chen and P. Technology, 2023, **311**, 123280.
12. Y. Li, T. Fan, W. Cui, X. Wang, S. Ramakrishna, Y. J. S. Long and P. Technology, 2023, **306**, 122586.
13. Y. Lu, H. Ma, F. Chen, Y. Zhao, L. Wen, C. Gao and L. J. J. o. M. S. Xue, 2023, 121419.
14. Y. Wang, C. Yuan, K. Zhou, Q. Gu, W. Jing, Z. Zhong and W. J. J. o. M. S. Xing, 2023, 121389.
15. C. Li, Y. Xiong, L. Zhao, H. Wan, J. Li, S. Fang, M. Wang, M. Duan, J. Ren and Y. J. L. Xiao, 2023.